3 INSTRUMENT

PICO meets all of its science-derived instrument requirements (STM) with a single instrument: an imaging polarimeter with 21 frequency bands centered between 21 and 799 GHz. The instrument is built around an all-aluminum two-reflector Dragone-style telescope (§3.1) with an internal aperture stop between the primary and secondary. The focal plane is populated by 12,996 transition edge sensor (TES) bolometers (§3.2) read out using a time domain multiplexing scheme (§3.3). The instrument utilizes a single science observing mode: fixed rotation rate imaging while scanning the sky.

A V-groove radiator assembly provides passive cooling (§3.4.3). The instrument is configured inside the shadow of the V-grooves, thermally and optically shielded from the Sun. The sun shadow cone depicted in Figure 3.1 is 29°. The angle to the Sun during the survey, □ = 26° (§4.1.2), is supplemented with a margin of 3° to account for the radius of the sun (0.25°), pointing control error, design margin, and alignment tolerances.

The V-groove assembly is attached to the bipod struts that support the instrument structural ring. The ring supports the primary reflector and telescope box. The telescope box contains the actively cooled components (§3.4.1, §3.4.2), including the secondary reflector, the focal plane and sub-K adiabatic refrigerator structures. Just inside the box, a thermal liner serves as a cold optical baffle and aperture stop.

During the survey, the instrument is spun at 1 rpm (§4.1.2). Spacecraft control is simplified by mounting the instrument on a spinning spacecraft module, while a larger non-spinning module houses most spacecraft subsystems (§4.3). Instrument elements that act as heat sources are accommodated on the spinning module of the spacecraft. Instrument integration and test (I&T) is described in §3.5.

3.1 Telescope

PICO telescope design is driven by a

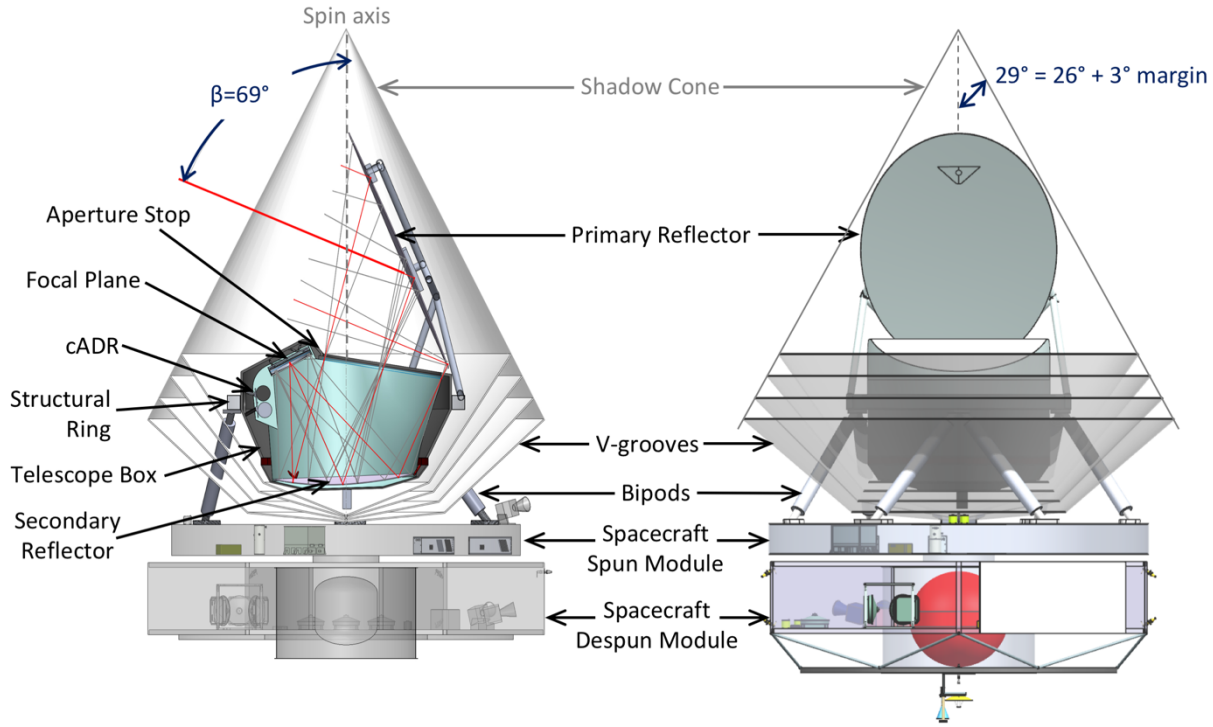

Figure 3.1: Detailed PICO instrument configuration shown. There are no moving or deployed parts. The spacecraft spun module accommodates warm instrument components: the 4K cooler compressor and drive electronics, the sub-K cooler drive electronics, and the detector warm readout electronics.

combination of science requirements and physical volume limits. The science requirements are: a large diffraction-limited field of view (DLFOV) sufficient to support ~10^4 detectors, arcminute resolution at 800 GHz and accurate polarization measurement with low sidelobe response. All requirements are met with PICO's 1.4 m aperture modified open-Dragone design (Figure 3.2). There are no moving parts

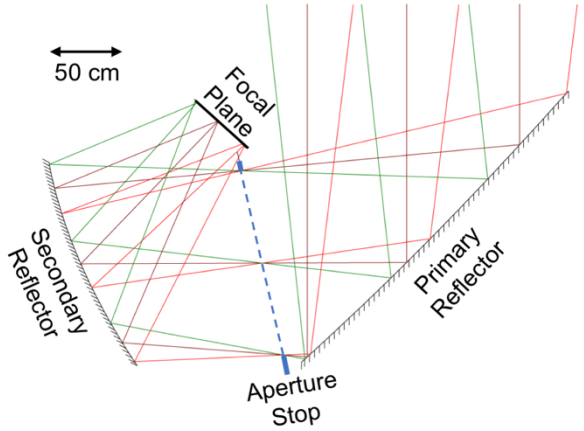

Figure 3.2: The optical system is compact.

in the PICO optical system.

More than 30 years ago Dragone analyzed the performance of several off-axis systems and found solutions with low cross-polarization at the center of the field of view and with stigmatism, or astigmatism and coma, canceled to first order (Dragone 1978) (Dragone 1983a) (Dragone 1983b). A number of recent suborbital CMB instruments have used off-axis systems, and several began design optimization with systems based on designs by Dragone (Fargant 2000, Swetz 2011, Padin 2008).

The PICO optical design was selected following a trade study examining cross-Dragone, Gregorian Dragone, and open-Dragone designs (Young 2018). The Gregorian Dragone has less diffraction-limited focal plane area than the open-Dragone (de Bernardis 2018), and is unable to support enough detectors to provide the required sensitivity. The cross-Dragone design has significant sidelobes that can be mitigated by baffles, but at the expense of added mass and volume.

Stray light analysis of the PICO open-Dragone design using GRASP confirms that the focal plane is protected from direct view of the sky (an advantage relative to the cross-Dragone system), that spillover past the primary is suppressed by 80 dB relative to the main lobe for both co-pol and cross-pol beams. Relative to the cross-Dragone, an open-Dragone also has a smaller f-number, so the volume constrained by the shadow cone can accommodate a larger effective aperture. The smaller f-number also reduces the physical focal plane size (for the same number of pixels), reducing focal plane mass and consequently the heat lift requirements on the active coolers (§3.4).

PICO's initial open-Dragone design follows Granet's method (Granet 2001), with f/1.42. An actively cooled circular aperture stop is added between the primary and secondary reflectors to reduce detector noise and shield the focal plane from stray radiation. Distortions are then added to the primary and secondary reflectors according to Dragone's published prescription (Dragone 1983b) to eliminate coma and increase the DLFOV. The detailed geometric parameterization of the PICO optical design is described in (Young 2018).

The two reflectors (270 cm x 205 cm primary and 160 cm x 158 cm secondary) are all-aluminum to minimize complexity. The highest frequency (900 GHz) sets the surface accuracy requirement of the reflectors to ~ $\lambda/14$=24 μm.

The slightly concave focal surface, which has a radius of curvature of 4.55 m, is telecentric to within 0.12° across the entire FOV. This results in a defocus of 0.1 mm at the edge of a flat 10 cm detector wafer, adding an RMS wavefront error of less than 3 μm, which is negligible relative to PICO's shortest wavelength.

3.2 Focal plane

Total	12,996	0.43	0.61	0.87	

Table 3.2: PICO measures in 21 broad overlapping frequency bands with band centers (ν_c) from 21 GHz to 799 GHz and bandwidths $\Delta\nu/\nu_c$ = 25%. The beams are single mode, with FWHM sizes of (6.2')*(155 GHz /ν_c). The Current Best Estimate

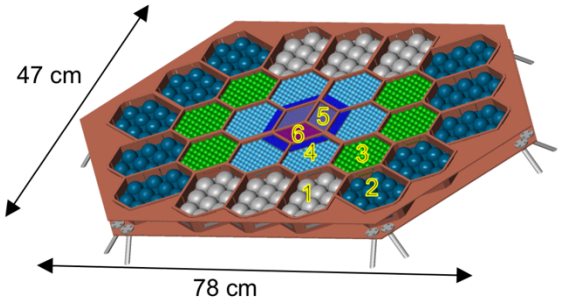

Figure 3.3: PICO focal plane. Detectors are fabricated on 6 types of tiles (shown numbered and colored to match first column in Table 3.1). The wafers are located on the focal plane such that higher frequency bands, which require better optical performance, are placed nearer to the center.

Tile type	N_{Tile}	Pixels / Tile	Pixel type	Bandcenters [GHz]	Sampling Rate [Hz]
1	6	10	A	21, 30, 43	45
2	10	10	B	25, 36, 52	55
3	6	61	C	62, 90, 129	136
4	6	85	D	75, 108, 155	163
		80	E	186, 268, 385	403
5	2	450	F	223, 321, 462	480
6	1	220	G	555	917
		200	H	666	
		180	I	799	

Table 3.1: PICO makes efficient use of the focal area with multichroic pixels (three bands per pixel, §3.2.1). The sampling rate is based on the smallest beam (Table 3.2), with 3 samples per FWHM at a scan speed (360°/min)sin(β=69°) = 336°/min.

PICO's focal plane is populated by an imaging array of transition edge sensor (TES) bolometers observing in 21 overlapping 25%-wide frequency bands with band centers ranging from 21-799 GHz. Polarization is measured by differencing the signals from pairs of polarization sensitive bolometers. A conceptual layout of the PICO focal plane is shown in Figure 3.3 and detailed in Table 3.1.

Modern mm/sub-mm detectors are photon noise limited, so the primary approach to increase sensitivity is to increase the number of detectors. The PICO focal plane has 12,996 detectors, 175 times the number flown on the Planck mission, providing a breakthrough increase in sensitivity with a comparably sized telescope. This breakthrough is enabled by development and demonstration by suborbital projects, which now commonly field arrays of ~10^4 detectors.

3.2.1 Low frequency detectors

PICO populates the majority of its FOV with multichroic pixels (MCPs) (Suzuki 2014, Datta 2014), which make optimal use of the focal plane area by feeding three photometric bands from a common broad-band antenna, with two single-polarization bolometers per band and therefore six bolometers per pixel.

Several competing optical coupling technologies have matured over the past ten years using horn-coupling (Duff 2016), antenna-array coupling (BICEP2 2015), and sinuous antenna/lenslet-coupling (Edwards 2012), delivering high optical efficiency over more than an octave of bandwidth. Pixel size, number, and spacing is relatively agnostic to the coupling scheme, so multiple options are open to PICO (technology maturation plan described in §5.2.1). For all of these schemes, microstrip mediates the signals between the antenna and detectors, and partitions the feed's wide continuous bandwidth into narrow channels using integrated micro-machined filter circuits (O'Brient 2013).

3.2.2 High frequency detectors

PICO's highest three frequency channels are beyond the Niobium superconducting band-gap, rendering microstrip filters a poor solution for defining the optical passband. In this regime, PICO instead measures a single band with each pixel using feedhorn-coupled polarization sensitive bolometers. Radiation is coupled through horns directly to the absorber coupled bolometers in the throat of a waveguide. The waveguide cut-off defines the lower edge of the band, and quasi-optical metal-mesh filters define the upper edge. Numerous experiments have successfully used similar approaches (Shirokoff 2011, Bleem 2012, Turner 2001). The technology maturation required for PICO is described in §5.2.1.

3.2.3 Sensitivity

We developed an end to end noise model of the PICO instrument to predict full mission sensitivity (Table 3.2) and provide a metric by which to evaluate mission design trades. The model considers four noise sources per bolometer: photon, phonon, TES Johnson, and readout (from both cold and warm readout electronics). To validate our calculations, we compared two independent software packages that have been used for several CMB instruments. The calculations agreed within 1% for both individual noise terms and for overall mission noise.

Laboratory experiments have demonstrated that TES detectors can be made background limited in the low loading environment they would experience at L2. For PICO, the primary contributor to noise is the optical load. The sources of optical load are the CMB, primary and secondary reflectors, aperture stop, and low pass filters. The CMB and stop account for the majority of the optical load at all frequencies. The CMB gives more than half the load in the middle and upper bands of the multichroic pixels, but the stop dominates the load in the lowest band of each pixel.

A more detailed description of the PICO noise model is available in (Young 2018). Small differences between Table 3.2 and the (Young 2018) quoted sensitivities are due to refinements of the component temperatures.

The sensitivity model assumes white noise at all frequencies, and does not include calibration uncertainties or estimates of other possible systematic effects, which are discussed in §2.7.

Sub-orbital submillimeter experiments have demonstrated TES detectors that are stable to at least as low as 20 mHz (Rahlin 2014), meeting PICO's requirements for the proposed scan strategy (§4.1.2).

3.3 Detector Readout

Suborbital experiment teams over the past ten years have chosen to use voltage biased TESs because their current readout scheme lends itself to SQUID based multiplexing. Multiplexing reduces the number of wires to the cryogenic stages and thus the total thermal load that the cryocoolers must dissipate. This approach also simplifies the instrument design.

In the multiplexing circuitry, SQUIDs

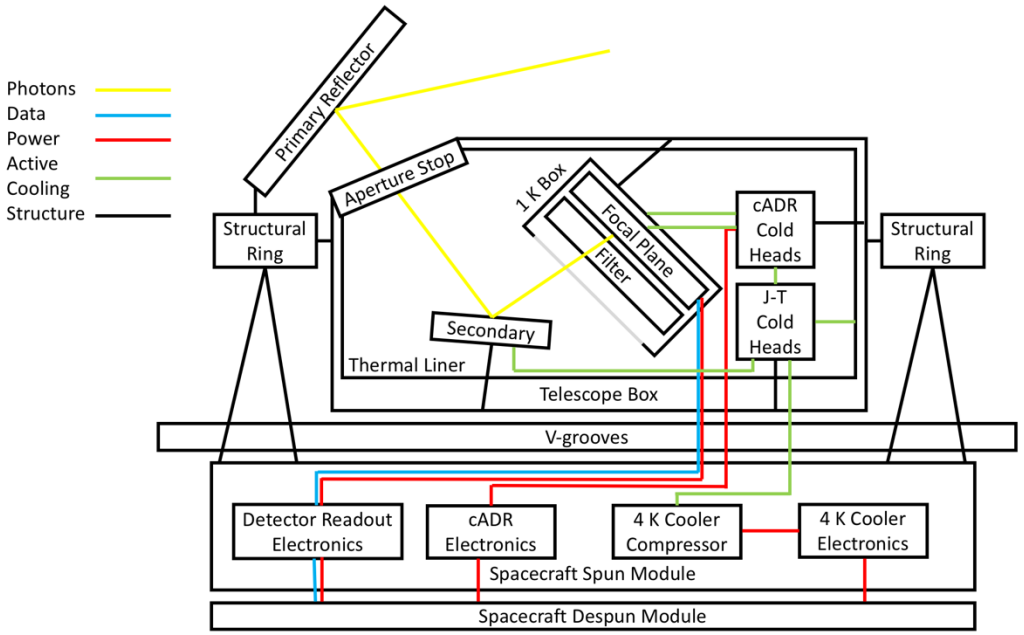

Figure 3.4: PICO instrument block diagram. Active coolers provide cooling to the focal plane, its box, the secondary reflector, and the thermal liner that acts as a cold aperture stop. Data from the focal plane flows to (redundant, cross-strapped) warm readout electronics on the spun module of the spacecraft bus.

function as low noise amplifiers and cryogenic switches. The current baseline for PICO is to use a time domain multiplexer (TDM), which assigns each detector's address in a square matrix of simultaneously read columns, and sequentially cycles through each row of the array (Henderson 2016). The PICO baseline architecture uses a matrix of 128 rows and 102 columns, requiring some technology maturation (§5.2.2). The thermal loading on the cold stages from the wire harnesses is subdominant to conductive loading through the mechanical support structures.

Redundant warm electronics boxes perform detector readout and instrument housekeeping using commercially available ASICs. The readout electronics compress the data before delivering it to the spacecraft. PICO detectors produce a total of 6.1 Tbits/day assuming 16 bits/sample, sampling rates from Table 3.1, and bolometer counts from Table 3.2. Suborbital work has demonstrated 6.2x compression of similar data (EBEX 2017). Planck HFI typically achieved 4.7x compression in flight (F. Pajot 2018, Planck HFI Core Team 2011). PICO conservatively assumes 4x.

Component	T Req'd	T CBE	Active heat lift		
			Req'd per model	Capability today	Projected capability
Primary reflector	< 40 K	17 K	N/A (radiatively cooled)		
Secondary reflector	< 8 K	4.5 K	42 mW total at 4.5 K		> 100 mW (§3.4.2, Figure 3.5)
Aperture stop	4.5 K				
cADR heat rejection	4.5 K				
Focal plane enclosure and filter	1.0 K	1.0 K	0.36 mW	1.0 mW	
Focal plane	0.1 K	0.1 K	5.7 uW	16 uW	

Table 3.3: Projected cooler heat lift capabilities offer >100% heat lift margin, complying with community best practices (Donabedian 2003). The cADR lift capability at 1 K and 0.1 K is from a Goddard quote. Both NGAS and Ball project >100 mW lift capability at 4.5 K using higher compression-ratio compressors currently in development (§3.4.2). The required loads were calculated using Thermal Desktop. (Ross 2004) was used to estimate the thermal conductive loads through mechanical supports. In addition to the listed components, the total 4.5 K heat load includes the intercept on the focal plane mechanical supports.

3.4 Thermal

Like the Planck-HFI instrument, PICO cools its focal plane to 0.1 K to enable detector operation (§3.4.1). To minimize detector shot noise due to instrument thermal radiation, the aperture stop and reflectors are cooled using both active and radiative cooling (§3.4.2, §3.4.3). All thermal requirements are met with robust margins (Table 3.3).

3.4.1 cADR Sub-K Cooling

A multi-stage continuous Adiabatic Demagnetization Refrigerator (cADR) cools the PICO focal plane to 0.1 K and the surrounding enclosure, filter, and readout components to 1 K. The cADR employs three refrigerant assemblies operating sequentially to absorb heat from the focal plane at 0.1 K and reject it to 1 K. Additionally, the cADR employs two assemblies operating sequentially to absorb this rejected heat at 1 K, cool other components to 1 K, and reject heat at 4.5 K. This configuration provides continuous cooling with small temperature variations at both the 0.1 K and 1 K. Heat straps connect the two cADR cold sinks to multiple points on the focal plane assembly, which has high thermal conductance paths built in, to provide spatial temperature uniformity and stability during operation. Heat loads in the range of 20 μW at 0.1 K and 1 mW at 1 K (time-average) are within the capabilities of current cADRs developed by GSFC (Shirron 2012) (Shirron 2016). The PICO sub-K loads are estimated at less than half of this capability.

3.4.2 4 K Cooler

A cryocooler system similar to that used on JWST to cool the MIRI detectors (Durand 2008, Rabb 2013) removes the heat rejected from the cADR and cools the aperture stop and secondary reflector to 4.5 K. Both NGAS (which provided the MIRI coolers) and Ball

Aerospace have developed such coolers under the NASA-sponsored Advanced Cryocooler Technology Development Program (Glaister 2006). NGAS and Ball use slightly different but functionally-equivalent hardware approaches. A 3-stage precooler (acoustic Stirling by NGAS or mechanical Stirling by Ball) provides ~16 K precooling to a separate circulated-gas loop driven by a similar compressor modified for DC flow. The circulated-gas loop utilizes Joule-Thomson (J-T) expansion, further cooling the gas to 4.5 K. The entire precooler assembly and the J-T circulator compressor are located on the warm spacecraft, with relatively short tubing lengths conducting the gas flow from the precooling point to the J-T expansion point. All waste heat rejected by the cooler compressors and drive electronics is transferred to the spacecraft heat rejection system. Unlike JWST, the PICO cooler does not require deployment of the remote cold head.

The J-T expansion point is located close to the cADR heat rejection point, thereby providing the lowest temperature to the cADR. Subsequent to cooling the cADR, the gas flow intercepts conducted heat to the focal plane enclosure, then cools the aperture stop and the secondary reflector before returning in counterflow to the circulation compressor.

Model-based projections indicate that the coolers delivered for MIRI could meet the PICO 4.5 K heat lift requirement with >100% margin with minimal changes: the replacement of the ^{4}He gas used for MIRI with ^{3}He, plus resizing of the gas counterflow heat exchangers to take advantage of the ^{3}He properties.

It is highly likely that a better solution will be available before Phase A. NGAS and Ball are actively working on increasing the flow rate and compression ratio of the J-T compressor, which should result in significantly higher system efficiency, and in greater heat lift margin above the PICO requirement. These improvements entail the implementation of well-known techniques (standard thermal engineering). The NGAS multi-stage J-T compressor has completed PDR-level development, and is

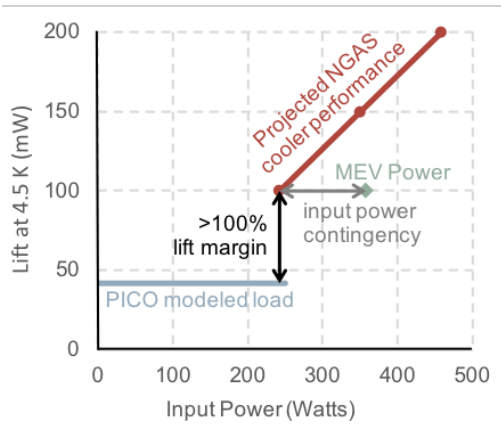

Figure 3.5: The projected performance of the NGAS cooler using a multi-stage compressor and 4He (Rabb 2013) meets PICO's requirements with >100% margin. PICO conservatively carries additional input power contingency on the efficiency of the cooler.

expected to reach CDR level well before needed for PICO. Projected performance is shown in Figure 3.5. The Ball approach started with a larger compressor, required less modification to achieve comparable performance, and eliminated the cold bypass-precooling valve that was problematic for MIRI. The Ball approach uses ^{3}He, while the NGAS approach uses ^{4}He. Both employ re-optimized gas heat exchangers (trivial engineering changes).

3.4.3 Radiative cooling

A set of four V-groove radiators provides passive cooling. The outermost of the four V-groove shields shadows the interior shields from the Sun. The V-grooves radiate to space, each reaching successively cooler temperatures. The V-groove assembly is mechanically supported from the spacecraft bus by attachment to the low-conductance bipod struts that also carry the mechanical loads of the structural ring (Figure 3.1). The V-groove assembly provides a cold radiative environment to the primary reflector, structural ring, and telescope box, so radiative loads on those elements are smaller than the conductive loads through the mechanical support structures.

3.5 Instrument Integration & Test

PICO Instrument I&T planning benefits greatly from heritage experience with the Planck HFI instrument (F. e. Pajot 2010).

PICO will screen detector wafer performance prior to selection of flight wafers and focal plane integration. The cADR and 4 K cryocooler will be qualified prior to delivery. The relative alignment of the two reflectors under thermal contraction will be photogrammetrically verified in a thermal vacuum (TVAC) chamber.

PICO will integrate the flight focal plane assembly and flight cADR in a dedicated sub-Kelvin cryogenic testbed. Noise, responsivity, and FPU temperature stability will be characterized using a representative optical load for each frequency band (temperature-controlled blackbody). Polarimetric and spectroscopic calibration will be performed.

The focal plane will be integrated with the reflectors and structures, and alignment verified photogrammetrically at cold temperatures in a TVAC chamber. The completely integrated observatory will be tested in TVAC to measure parasitic optical loading from the instrument, noise, microphonics and radio-frequency interference (RFI).

4 Design Reference Mission

4.1 Concept of Operations

The PICO concept of operations is similar to that of the successful WMAP (Bennett 2003) and Planck (Tauber 2010) missions. After launch, PICO cruises to a halo orbit around the Earth-Sun L2 Lagrange point (§4.1.1). En route, a 2-week decontamination period is followed by instrument cooldown. After in-orbit checkout is complete, PICO begins the science survey.

PICO has a single science observing mode, surveying the sky continuously for 5 years using a pre-planned repetitive survey pattern (§4.1.2). Instrument data are compressed and stored on-board, then returned to Earth in daily 4-hr Ka-band science downlink passes (concurrent with science observations). Because PICO is observing relatively static galactic, extragalactic, and cosmological targets, there are no requirements for time-critical observations or data latency. Presently, there are no plans for targets of opportunity or guest observer programs during the prime mission. The PICO instrument does not require cryogenic consumables (as the Planck mission did), permitting consideration of mission extension beyond the prime mission.

4.1.1 Mission Design and Launch

PICO performs its science survey from a halo orbit around the Earth-Sun L2 Lagrange point. Predecessor missions Planck and WMAP both operated in L2 orbits.

L2 orbits provide favorable survey geometry (relative to Earth orbits) by mitigating viewing restrictions imposed by terrestrial and lunar stray light. The PICO orbit around L2 is small enough to ensure than the Sun-Probe-Earth (SPE) angle is less than 15°. This maintains the telescope boresight >70° away from the Earth (Figure 4.2, 70°=180°-α-□ -SPE).

High data rate downlink to the Deep Space Network (DSN) is available from L2 using near-Earth Ka bands. L2 provides a stable thermal environment, simplifying thermal control. The PICO orbit exhibits no post-launch eclipses.

NASA requires that Probes be compatible with an Evolved Expendable Launch Vehicle (EELV). For the purpose of this study, the Falcon 9 (SpaceX 2015) is used as the reference vehicle. Figure 4.1 shows PICO configured for launch in a Falcon 9 fairing. PICO's launch mass is well within the Falcon 9 capability.

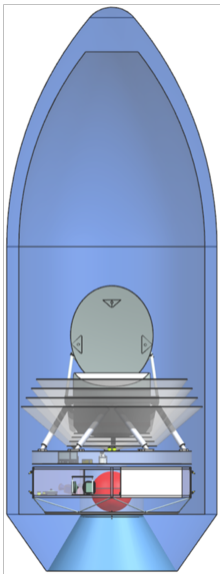

Figure 4.1: PICO is compatible with the Falcon 9.

Insertion to the halo manifold and associated trajectory correction maneuvers (TCMs) require 150 m/s of total Δv by the spacecraft. The orbital period is ~6 months. Orbit maintenance requires minimal propellant (statistical Δv ~2 m/s per year). There are no disposal requirements for L2 orbits, but spacecraft are customarily decommissioned to heliocentric orbit.

4.1.2 Survey Design

PICO utilizes a highly repetitive scan strategy to map the full sky. During the survey, PICO spins with a period T_{spin} = 1 min about a spin axis oriented α=26° from the anti-solar direction (Figure 4.2). This spin axis is forced to precess about the anti-solar direction with a period T_{prec}= 10 hr. The telescope boresight is oriented at an angle □ =69° away from the spin

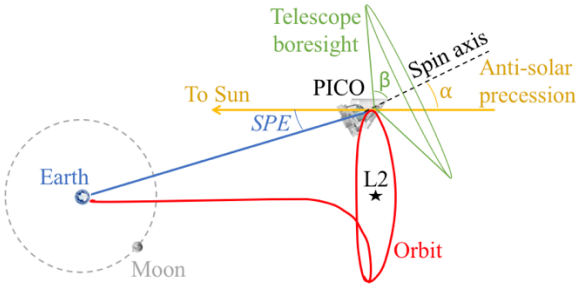

Figure 4.2: PICO surveys by continuously spinning the instrument about a precessing axis.

axis. This □ angle is chosen such that $\alpha+\square > 90°$, enabling mapping of all ecliptic latitudes. The precession axis tracks with the Earth in its yearly orbit around the Sun, so this scan strategy maps the full sky (all ecliptic longitudes) within 6 months.

PICO's $\alpha=26°$ is chosen to be substantially larger than the Planck mission's α angle (7.5°) to mitigate systematic effects by scanning across each sky pixel with a greater diversity of orientations (Hu 2003). Increasing α further would decrease the sun-shadowed volume available for the optics and consequently reduce the telescope aperture size. A deployable sun shade was considered, but not baselined.

The instrument spin rate, selected through a trade study, matches that of the Planck mission. The study balanced low frequency (1/f) noise subtraction (improves with spin rate) against implementation cost and heritage, pointing reconstruction ability (anti-correlated with spin rate), and data volume (linearly correlated with spin rate). The ℓ=2 quadrupole power spectral mode appears in the data timestream at $2\ell \sin(\square)/T_{spin}$ = 60 mHz (Wallis 2017). Detector noise is stable down to these frequencies (§3.2.3). A destriping mapmaker applied in data post-processing effectively operates as a high-pass filter, as demonstrated by Planck (Kurki-Suonio 2009). PICO's spin axis precession frequency is >400x faster than that of Planck, greatly reducing the effects of any residual 1/f noise by spreading the effects more isotropically across pixels.

4.2 Ground Segment

The PICO Mission Operations System (MOS) and Ground Data System (GDS) can be built with extensive reuse of standard tools. The PICO concept of operations is described in §4.1. There are no time critical events, and no driving data latency requirements. Routine orbit maintenance activities are required roughly every three months (§4.1.1). The payload consists of a single instrument with a single science observing mode (a repetitive survey pattern, §4.1.2).

All space-ground communications, ranging, and tracking are performed by the Deep Space Network (DSN) 34 m Beam Wave Guide (BWG). X-band is used to transmit spacecraft commanding, return engineering data, and provide navigation information. Ka-band is used for high rate return of science data (150 Mb/s transfer; 130 Mb/s information rate after CCSDS encoding). The instrument produces 6.1 Tb/day, which is compressed to 1.5 Tb/day (§3.3). Daily 4 hr DSN passes return PICO data in 3.1 hr, with the remaining 0.9 hr available as needed for retransmission or missed pass recovery.

4.3 Spacecraft

The PICO spacecraft bus meets all performance requirements with margin. It is designed for a minimum lifetime of 5 years in the L2 environment. Mission critical elements are redundant. Flight spares, engineering models and prototypes appropriate to Class B are budgeted.

The aft end of the spacecraft (the "de-spun module") is comprised of six equipment bays that house standard components (Figure 4.3). The instrument and V-grooves are mounted on bipods from the spacecraft "spun module," which contains hosted instrument elements (Figure 3.1). A spin motor drives the spun module at 1 rpm to support the science survey requirements (§4.1.2). Reaction wheels on the despun module cancel the angular momentum of the spun module and provide three-axis control (§4.3.1).

The bipods that mechanically support the instrument are thermally insulating. The passively radiating V-groove assembly thermally isolates the instrument from solar radiation and from the bus (§3.4.3). Like Planck (Tauber 2010), the V-grooves are manufactured using honeycomb material. Additional radiators on the spun and despun spacecraft modules (~1 m^2 each) reject heat dissipated by spacecraft subsystems and hosted instrument elements.

PICO's avionics are dual-string with standard interfaces. Solid state recorders provide

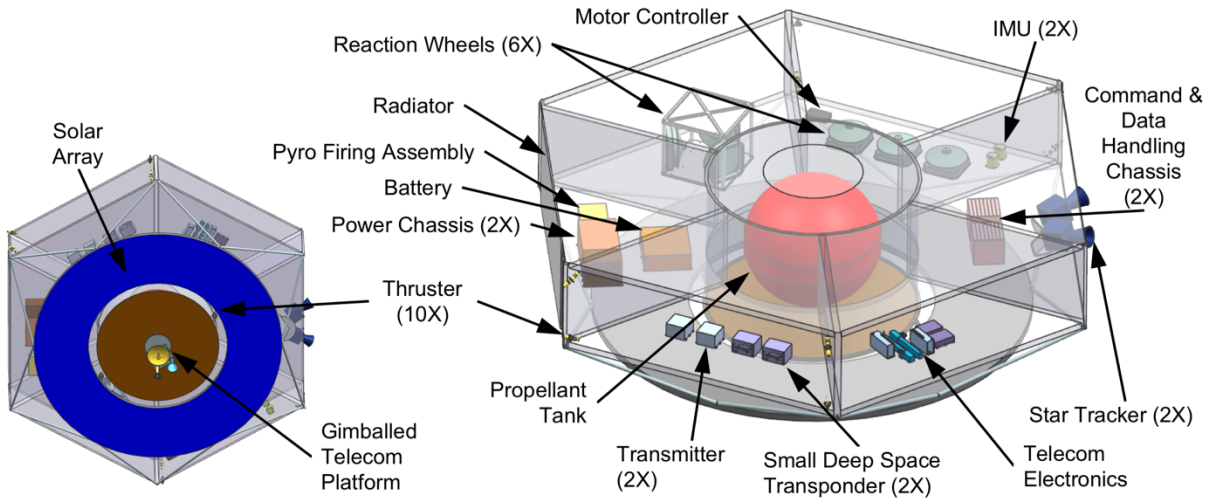

Figure 4.3: Modular equipment bays provide easy access to all components in the spacecraft de-spun module and enable parallel integration of spacecraft subsystems.

three days of science data storage (ensuring robustness to missed telecom passes).

PICO employs a fully redundant Ka- and X-band telecommunications architecture. The Ka-band system uses a 0.3 m high gain antenna to support a science data downlink information rate of 130 Mbps to a 34 m BWG DSN ground station with a link margin of 4.8 dB. The X-band system provides command and engineering telemetry communication through all mission phases using medium and low gain antennas. Amplifiers, switches, and all three antennas are on a gimballed platform, enabling Ka and X-band downlink concurrent with science observations.

Solar cells on the aft side of the bus provide positive power (with contingency) for all mission power modes after launch. The driving mode is telecom concurrent with science survey. Unused area in the solar array plane affords significant margin for growth (Figure 4.3). A Li-Ion battery provides power during the launch phase. The heritage power electronics are dual string.

The propulsion design is a simple monoprop blow-down hydrazine system with standard redundancy. Two aft-pointed 22 N thrusters provide Δv and attitude control for TCMs and orbit maintenance. Eight 4 N thrusters provide momentum management and backup attitude control authority.

4.3.1 Attitude Determination & Control

PICO uses a zero net angular momentum control architecture with heritage from the SMAP mission (Brown 2016). PICO's instrument spin rate (1 rpm) matches that of the Planck mission, but the precession of the spin axis is much faster (10 hr vs 6 months), and the precession angle much larger (26° vs 7.5°). These differences make the spin-stabilized Planck control architecture impractical because of the amount of torque required to drive precession.

The PICO 1 rpm instrument spin rate is achieved and maintained using a spin motor. The spin motor drive electronics provide the coarse spin rate knowledge used for controlling the spin rate to meet the ±0.1 rpm requirement.

Three reaction wheel assemblies (RWAs) are mounted parallel to the instrument spin axis and spin opposite to the instrument to achieve zero net angular momentum and keep the despun module three-axis stabilized. The spin axis is precessed using three RWAs mounted normal to the spin axis in a triangle configuration. Each set of three RWAs is sized such that two could perform the required function, providing single fault tolerance.

Spin axis pointing and spin rate knowledge are achieved and maintained using star tracker and inertial measurement unit (IMU) data. The attitude determination system is single fault tolerant, with two IMUs each on the spun and despun modules, and two star trackers each on the spun and despun modules. Two sun sensors on the despun module are used for safe mode contingencies and instrument Sun avoidance. All attitude control and reconstruction requirements are met, including spin axis control < 60 arcmin with < 1 arcmin/min stability, and reconstructed pointing knowledge < 10 arcsec (each axis, 3σ).

5 TECHNOLOGY MATURATION

PICO's detector and readout technologies have already been substantially matured through complimentary suborbital experiments, and can be developed by the APRA and SAT programs to NASA's Technology Readiness Level (TRL) 5 before Phase A (October 2023). The 4 K cryocooler baselined by PICO requires only standard thermal engineering (§3.4.2).

5.1 Current State of Technologies

PICO builds off of the heritage of the Planck HFI instrument. The white noise of the Planck NTD-Ge bolometers was background limited in all channels (Planck 2014) with a 1/f knee at 200-300 mHz (Planck 2018). Since Planck, numerous suborbital experiments have used monolithically fabricated TES bolometers and multiplexing schemes to field instruments with thousands of detectors per camera.

5.1.1 Detectors status

Suborbital teams have successfully demonstrated a variety of optical coupling schemes, including horns with ortho-mode transducers (OMTs), lithographed antenna arrays, and sinuous antennas under lenslettes (Figure 5.1). They have achieved background limited performance in both ground and balloon instruments. Experiments have covered many of PICO's observing bands between 30 GHz and 270 GHz (Table 5.1). SPT-3G has used the PICO-baselined three-color pixel design to deploy 16,260 detectors covering 90-150-220 GHz. Other experiments have successfully deployed two-color pixels. All of these detector arrays have been packaged into modules and focal plane units in working cameras representative of the PICO integration.

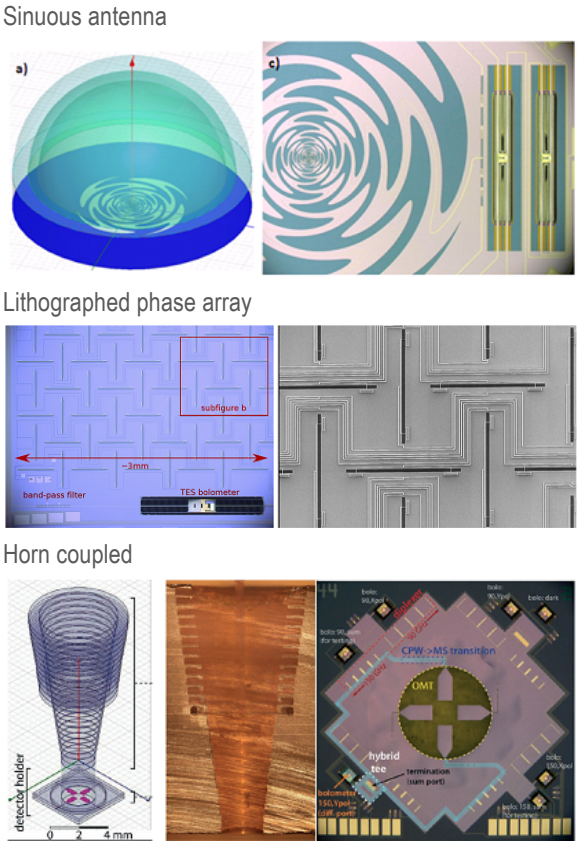

Figure 5.1: Multiple demonstrated optical coupling schemes are available to PICO. Images from CMB-S4 Technology Book (Abitbol 2017).

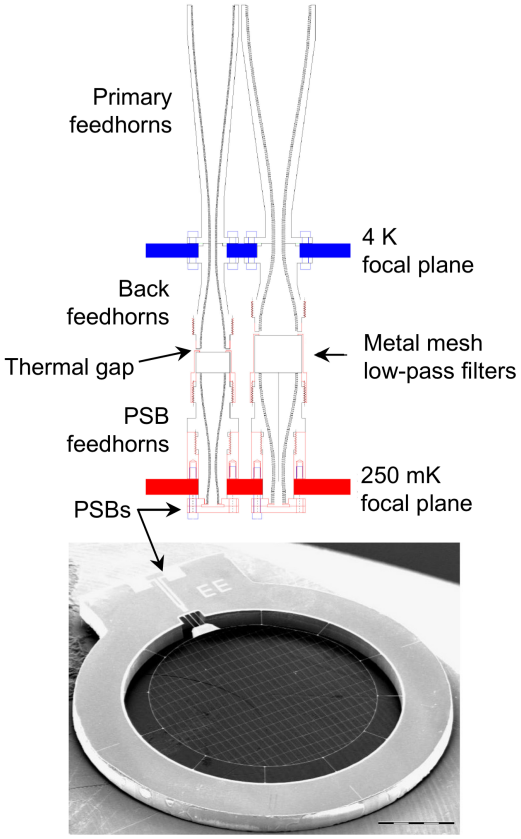

Figure 5.2: Direct-absorbing dual-polarized detectors and coupling horns used in Planck for 143-343 GHz bands.

To date, suborbital experiments have achieved statistical map depths of 3 uK_{CMB}-arcmin on degree-scaled modes over small parts of the sky, approaching what PICO will achieve over the entire sky. Suborbital experiments have also demonstrated systematic control to this level through full-pipeline simulations and null-test analysis (jackknife tests). Moreover, laboratory tests and in-flight data from balloons suggest that these TES bolometers are more naturally robust against cosmic rays than the individual NTD-Ge bolometers used in Planck. Cosmic ray glitches have fast recovery times and low coincidence rates (SPIDER 2018).

PICO's 555-799 GHz channels (above the Niobium band gap) will use direct absorber bolometers. Ground and balloon experiments have deployed focal planes with hundreds of horn-coupled spiderweb bolometers. SPT-Pol deployed dual-polarized versions of direct absorber horn-coupled bolometers. Planck used this style of bolometer, but with NTD-Ge thermistors instead of TESes (Figure 5.2). Filled arrays of detectors such as Backshort Under Ground (BUG) bolometers are also an option for these channels. The status of these efforts is summarized in Table 5.1.

5.1.2 Readout electronics status

More than 10 experiments have used TDM readout. SCUBA2 on JCMT has 10,000 pixels, nearly as many detectors as planned for PICO (Holland 2013).

5.2 Development Plan

5.2.1 Detector Development

The baseline PICO instrument requires three-color dual-polarized antenna-coupled bolometers covering bands from 21-462 GHz and single-color dual-polarized direct-absorbing bolometers from 555-799 GHz (§3.2.1, Table 3.1). The developments required to enable the PICO baseline design are:

- Extension of antenna-coupled bolometers down to 21 GHz and up to 462 GHz
- Demonstration of three-color pixels across that spectrum, with characterization of beam properties and associated systematics
- Construction of high frequency direct absorbing arrays and laboratory testing
- Beam line and 100 mK testing to simulate the cosmic ray environment at L2

The extension to lower frequencies requires larger antennas and therefore control of film properties and lithography over larger areas. Scaling to higher frequencies forces tighter critical dimensions and materials tend to exhibit higher losses. These challenges require tight control of cleanliness and full understanding of process parameters.

The sinuous antenna has the bandwidth to

Project	Type	Polarized	Mono-lithic	$\nu_{c,Low}$ [GHz]	$\nu_{c,High}$ [GHz]	Colors per pixel	N_{bolo}	Significance	Reference
PICO low frequency	**Probe**	**Yes**	**Yes**	**21**	**462**	**Three**	**11,796**		**§3.2.1**
SPT-3G	Ground	Yes	Yes	90	220	Three	16,260	Trichroic	(Anderson 2018)
Advanced ACT-pol	Ground	Yes	Yes	27	230	Two	3,072	Dichroic	(Simon 2018)
BICEP/Keck	Ground	Yes	Yes	90	270	One	5,120	50nK-deg	(BICEP2&Keck 2018)
Berkeley, Caltech, NIST	Lab	Yes	Yes	30	270	Two	NA	Band coverage	
SPIDER	Balloon	Yes	Yes	90	150	One	2,400	Stable to 10mHz	(Rahlin 2014)
PICO high frequency	**Probe**	**Yes**	**Yes**	**555**	**799**	**One**	**1,200**		**§3.2.2**
Planck HFI	Flight	143-343 GHz	No	143	857	One	48	TRL 9 absorbing bolometers	(Planck HFI Core Team 2011)
SPT-SZ	Ground	No	Yes	90	220	One	840	Monolithic array TESes	
SPT-pol-90	Ground	Yes	No	90	90	One	180	Dual pol absorbing TESes	

Table 5.1: Multiple active suborbital efforts are advancing technologies relevant to PICO

service three-colors per pixel, whereas horns and antenna arrays have only been used for two, so some version of the sinuous antenna will likely be needed to realize three-color pixels. However, the sinuous antenna couples to states that "wobble" log-periodically with frequency. There are potential solutions to this in the focal plane design, analysis, and free parameters of the antenna geometry. These will need to be explored subject to the uniformity and packing density constraints present at the extreme spectral bands. Systematics studies for field demonstrations will be particularly important. The PICO concept is robust to any challenges in developing three-color pixels; §5.3 describes an option to descope to two-color pixels.

Planck demonstrated the architecture of horns coupled to direct absorbing bolometers. For PICO's high frequency detectors, this only needs to be generalized to dual polarized arrays. The greatest remaining challenge is the low risk development of a packaging design. Such prototyping could culminate in a field demonstration, best performed in a balloon.

So far, cosmic ray tests and in-flight analysis of TES bolometers are encouraging (SPIDER 2018). The CMB community can retire residual risk with 100 mK testing where the array heat sinking may be weaker, and beam-line tests to help control for background glitch rates.

A plan to accomplish all required development is described in Table 5.2.

5.2.2 Readout Electronics Development

PICO's sensitivity requirements dictate the use of ~13,000 transition edge sensor bolometers, requiring a highly multiplexed system. The PICO baseline design calls for time division multiplexing with 128 switched rows per readout column (TDM-128x), which exceeds that of Advanced ACTPol's recently demonstrated TDM-66x (Henderson 2016). The leap to TDM-128x requires:

- Development of fast-switched room temperature electronics
- System engineering of room temperature to cryogenic row select cabling to ensure sufficiently fast row switch settling times
- Demonstration of TDM-128x SQUID aliased noise below PICO detector sensitivity requirements

A plan to accomplish the required development is described in Table 5.2.

5.3 Technology Descopes

A descope from three-color to two-color pixels remains a viable alternative should the three-color technology not mature as planned. Descope studies suggest that a PICO-size focal plane using two-color pixels at the lower frequencies and the baseline one-color pixels at

Task	Current status	Milestone A	Milestone B	Milestone C	Current Funding	Required Funding	Date TRL5 achieved
3-color arrays ν<90 GHz	See Table 5.1	Field demo of 30-40 GHz (2020)	Lab demos 20-90 GHz (2022)		APRA & SAT funds	$2.5M over 4 yr (1 APRA +1 SAT)	2022
3-color arrays ν>220 GHz		Field demo of 150-270 GHz (2021)	Lab demos 150-460 GHz (2022)		APRA & SAT funds	$3.5M over 4 yr (2 SATs)	2022
Direct absorbing arrays ν>550 GHz		Design & prototype of arrays (2021)	Lab demo of 555 GHz (2022)	Lab demo 799 GHz (2023)	None	$2M over 5 yr (1 SAT)	2023
Cosmic ray studies	250 mK w/ sources	100 mK tests with sources (2021)	Beamline tests (2023)		APRA & SAT funds	$0.5-1M over 5 yr (part of 1 SAT)	NA
Fast readout electronics	MUX66 demo	Engineering and Fab of electronics (2020)	Lab demo (2021)	Field demo (2023)	No direct funds	$2.5M over 5 yr (1 SAT)	2023
System engineering/ 128x MUX demo	MUX66 demo	Design of cables (2020)	Lab demo (2021)	Field demo (2023)	No direct funds		

Table 5.2: PICO technologies can be developed to TRL 5 prior to a 2023 Phase A start using the APRA and SAT programs

the higher frequencies would contain 8,840 detectors (compared to the baseline 12,966) and map in 19 colors (baseline 21). Because horns have a 2.3:1 bandwidth, each of the two bands in a pixel has 35% bandwidth (compared to the baseline 25%), which compensates for pixel count, resulting in the same 0.61 uK_{CMB}-arcmin aggregate map depth (Table 3.2), but with coarser spectral resolution.

5.4 Enhancing Technologies

The following technologies are neither required nor assumed by the PICO baseline concept. They represent opportunities to extend scientific capabilities or simplify engineering.

PICO baselines TDM readout because of its relative maturity and demonstrated sensitivity and stability in relevant science missions. Lab tests of Frequency Domain Multiplexing (FDM) suggest comparable performance with higher multiplexing factors and lower loads on cryogenic stages relative to TDM. Suborbital experiments such as SPT-3G have used frequency division multiplexing (FDM) to readout focal planes comparable in size to PICO.

Microwave frequency SQUID multiplexing can increase the multiplexing density and reduce the number of lines between the 4K and ambient temperature stages (Dober 2017, Irwin 2004). Kinetic Inductance Detectors (KIDs) and Thermal KIDs (TKIDs) can further reduce the wire count, obviate the SQUIDs, and dramatically simplify integration by performing multiplexing on the same substrate as the detectors themselves (McCormick 2016, Steinbach 2018). The cost to develop these technologies is $3-4M/year, with a high chance of reaching TRL-5 before Phase A.

6 Project Management, Heritage, Risk, and Cost

6.1 PICO Study Participants

The PICO study was open to the entire mm/sub-mm science community and included more than 150 scientists. Seven working groups were led by members of PICO's Executive Committee, which met weekly under the leadership of PI Shaul Hanany. More than 60 people participated in-person in two community workshops (November 2017 and May 2018).

The PICO engineering concept definition package was generated by Team X (the JPL concurrent design lab). The Team X study was supported by inputs from a JPL engineering team and Lockheed Martin.

The full list of study report contributors and endorsers follows the cover page.

6.2 Project Management Plan

PICO benefits from the experience of predecessor missions such as Planck and WMAP, as well as many years of investment in technology development and a multitude of suborbital experiments. In addition to demonstrated science and engineering capabilities, this heritage has developed a community of people with the expertise required to field a successful mission.

This study assumes mission management by JPL with a Principal Investigator leading a single science team. A Project Manager provides project oversight for schedule, budget, and deliverables. A Project Systems Engineer leads systems engineering activities and serves as the Engineering Technical Authority. A Mission Assurance Manager serves as the Independent Technical Authority. The PICO mission development schedule is shown in Figure 6.1.

Probes are medium-class missions, similar in cost scope to NASA's *New Frontiers* missions, which are Category 1 and Risk Classification A or B, with Phase A-D costs capped at ~$850M (not including the launch vehicle). JPL is well-prepared to manage Probe missions, having managed the Juno *New Frontiers* mission (launched 2011) and also the development of the medium-class Spitzer Space Telescope (launched 2003). JPL delivered the bolometric detectors for the Planck HFI instrument (launched 2009). Presently, JPL is managing NEOCam, a *Discovery* class infrared space telescope.

The PICO spacecraft provider will be selected during mission formulation. Multiple organizations are capable of providing a spacecraft bus to meet PICO's requirements. Lockheed Martin contributed to the PICO concept study, leveraging their experience with *New Frontiers* missions Juno and OSIRIS-REx.

6.3 Heritage

The successful Planck mission provides science heritage for PICO. Technical heritage traces to multiple missions.

Because PICO observes in the mm/sub-mm regime, the surface accuracy requirement for the reflectors is relatively easy to meet. PICO's reflectors are similar to Planck's, but somewhat larger (270 x 205 cm primary vs. 189 cm x 155 cm) (Gloesener 2006). Herschel observed at wavelengths more demanding than PICO's and was larger (350 cm diameter primary) (Toulemont 2004).

The heritage of the PICO detectors and readout electronics (§3.2,3.3) is described in

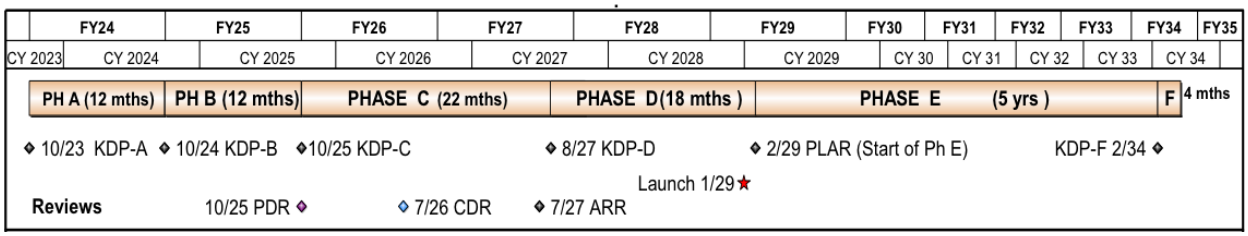

Figure 6.1: The PICO baseline schedule is based on historical actuals from similarly-sized missions such as Juno and SMAP.

§5.1.

PICO's detectors are cooled by a cADR (§3.4.1) with requirements that are within the capabilities of current cADRs developed by Goddard Space Flight Center. These systems have been applied to several JAXA missions, including Hitomi (Shirron 2016).

PICO's 4 K cryocooler (§3.4.2) is a direct extension of the JWST MIRI design (Durand 2008, Rabb 2013). PICO benefits from a simpler and more reliable implementation of the J-T system than was required for MIRI, in that no deployment of cooling lines is required, and all flow valving is performed on the warm spacecraft. Cooling multiple independent points with a J-T loop has been demonstrated on Planck with the JPL-supplied 18 K cooler (Planck 2011).

Structures similar to PICO's V-groove assembly (§3.4.3) are a standard approach for passive cooling first described more than thirty years ago (Bard 1987). The JWST mission will deploy a 22 m x 10 m V-groove sun shield. PICO's relatively modest 4.5 m diameter V-groove assembly fits inside the launch vehicle fairing. Because it doesn't require deployment, PICO has baselined a simple honeycomb material construction like that successfully flown by the Planck mission (ESA 2009) (Planck 2011).

Most requirements on the PICO spacecraft are well within typical ranges and can be met with standard high heritage systems (§4.3). PICO's spin architecture and data volume requirements are less typical, and discussed below.

The PICO zero-momentum control architecture (§4.3.1) has heritage from the SMAP mission. PICO has a slower spin rate and less cancelled angular momentum than SMAP. SMAP requires 359 Nms to cancel the momentum of a 6 m instrument antenna spun at 14.6 rpm (Brown 2016). The PICO launch mass (including contingency) is similar to the Planck launch mass. If we assume Planck moments of inertia (ESA 2016), the PICO spun elements would have an angular momentum of 210 Nms at 1 rpm. This is conservative because, unlike Planck, the entire PICO observatory doesn't spin.

Though PICO's data volume is notable by current standards, it is already enveloped by missions in development. PICO produces 6.1 Tb/day of raw data which is compressed to 1.5 Tb/day (§3.3). PICO downlinks data daily, but baselines storage of 3 days of (compressed) data to mitigate missed telecom passes. This requires 4.5 Tb of onboard storage, in family with the 3.14 Tb solid state recorder currently in use by Landsat 8 and much smaller than the 12 Tbit flash memory planned for NISAR (Jasper 2017). The PICO baseline 150 Mb/s Ka-band data downlink is an existing DSN catalog service (DSN 2015). The TESS mission presently downlinks data to the DSN using Ka-band at 100 Mb/s. The baseline PICO mission generates ~2,200 Tb of raw (uncompressed) data per year, less than the ~6,800 Tb/year currently returned by Landsat 8 and ~9,300 Tb/yr planned by NISAR (Jasper 2017).

6.4 Risk Assessment

6.4.1 Pre-Mission Risks

Technology development (§5) is performed prior to the beginning of mission development, and is outside of the mission cost (per NASA direction), so associated risks do not represent threats to the cost of mission development. Rather, they represent risks to the availability of the described baseline mission. A technology-related mission descope is described in §5.3.

6.4.2 Development Risks

PICO's healthy contingencies, margins, and reserves provide flexibility to address risks realized during mission development. PICO carries >40% instrument sensitivity margin (Table 3.2), >100% heat lift margin (Table 3.3), 43% system power contingency, 31% payload mass contingency, and 27% spacecraft mass contingency. The Falcon 9 launch capability (for ocean recovery) exceeds PICO's total launch

mass (including contingency) by a ~50% margin. The PICO budget includes 30% cost reserves for Phases A-D (§6.5).

During mission development the Project Systems Engineer continually assesses risks, tracks progress toward retiring them, and updates mitigations. Mitigations for a few top risks identified during this study are described below.

Thermal risk can be mitigated through extensive thermal modeling and review in Phase A, and design for early test verification. Risks associated with the instrument spin architecture can be mitigated by engaging JPL engineers who were involved in the SMAP mission. Detector delivery schedule risk can be mitigated by beginning fabrication early in the project life cycle and fabricating a generous number of detector wafers to ensure adequate yield. Risks associated with the integration and test of a cryogenic instrument can be mitigated through advanced planning and allocation of appropriate schedule and schedule margin.

6.4.3 Operations Risks

The PICO design meets the requirements associated with the NASA Class B risk classification. For Class B missions, essential spacecraft and instrument functions are typically fully redundant. This increases mission cost, but significantly reduces the risk of mission failure during operations.

The PICO mission utilizes a single instrument with a single observing mode mapping the sky using a repetitive survey pattern. The mission does not require any time-critical activities. The observatory fits in to the launch vehicle fairing in its operational configuration, so no hardware deployments are required. The telescope does not require a cover (nor the associated mission-critical cover release).

The spacecraft incorporates a fault protection system for anomaly detection and resolution. The Sun-pointed, command receptive, thermally stable safe-mode attitude allows ground intervention for fault resolution without time constraints. PICO's high degree of hardware redundancy and onboard fault protection ensure spacecraft safety in the event of unforeseen failures and faults.

Science data analysis, including foreground separation (§2.5) and systematics control (§2.6) are discussed in the science section (§2).

6.5 Mission Cost

The cost section is excluded from this draft release

7 BIBLIOGRAPHY

Abitbol, M. H., et al. 2017. "CMB-S4 Technology Book, First Edition." *arXiv:1706.02464.*

Anderson, A. J., et al. 2018. "SPT-3G: A Multichroic Receiver for the South Pole Telescope." *Journal of Low Temperature Physics* https://doi.org/10.1007/s10909-018-2007-z.

Bard, S. 1987. "Development of a high-performance cryogenic radiator with V-groove radiation shields." *J. of Spacecraft and Rockets* 24 (3): 193-197.

Bennett, C. L., et al. 2003. "The Microwave Anisotropy Probe (MAP) Mission." *ApJ* 583: 1.

Benson, B., et al. 2014. "SPT-3G: A Next-Generation Cosmic Microwave Background Polarization Experiment on the South Pole Telescope." *Proceedings of SPIE.*

BICEP2&Keck. 2018. "BICEP2 / Keck Array X: Constraints on Primordial Gravitational Waves using Planck, WMAP, and New BICEP2/Keck Observations through the 2015 Season." *Submitted to Phys. Rev. Lett.*

BICEP2, SPIDER, and Keck Array collaborations, et al. 2015. "Antenna-coupled TES Bolometers used BICEP2, Keck Array, and SPIDER." *ApJ* (912 No. 2).

Bleem, L. et al. 2012. "An Overview of the SPTpol Experiment." *J. Low Temp. Phys.* 167: 859-864.

Brown, T. S. 2016. "A GNC Perspective of the Launch and Commissioning of NASA's SMAP (Soil Moisture Active Passive) Spacecraft." 54th AIAA Aerospace Sciences Meeting.

Datta, R., Hubmayr, J., Munson, C., et al. 2014. "Horn Coupled Multichroic Polarimeters for the Atacama Cosmology Telescope Polarization Experiment." *Journal of Low Temperature Physics* (176): 670–676.

de Bernardis, P., Ade, P. A. R., Baselmans, J. J. A., et al. 2018. "Exploring cosmic origins with CORE: The instrument." *Journal of Cosmology and Astro-Particle Physics* 2018: 015.

de Haan, T. et al. 2012. "Improved Performance of TES Bolometers using Digital Feedback." *Proc. SPIE.*

Dobbs, M., Bissonnette, E., and Spieler, H. 2007. "Digital frequency domain multiplexer for mm-wavelength telescopes." *15th IEEE-NPSS Real-Time Conference.*

Dober, B. et al. 2017. "Microwave SQUID Multiplexer demonstration for Cosmic Microwave Background Imagers." *Appl. Phys. Let.* 111.

Donabedian, M., ed. 2003. *Spacecraft Thermal Control Handbook, Volume 2: Cryogenics.* The Aerospace Corporation.

Dragone, C. 1983a. "First-order correction of aberrations in Cassegrainian and Gregorian antennas." *IEEE Transactions on Antennas and Propagation* 31: 764-775.

Dragone, C. 1978. "Offset multireflector antennas with perfect pattern symmetry and polarization discrimination." *Bell Labs Technical Journal* 57 (7): 2663-2684.

Dragone, C. 1983b. "Unique reflector arrangement with very wide field of view for multibeam antennas." *Electronics Letters* 19 (25): 1061-1062.

DSN. 2015. "Deep Space Network Services Catalog 820-100, Rev. F." February 24. https://deepspace.jpl.nasa.gov/files/820-100-F1.pdf.

Duff, S., et al. 2016. "Advanced ACTPol Multichroic Polarimeter Array Fabrication Process for 150 mm Wafers." *J. of Low Temp. Phys.* 184.

Durand, D. et al. 2008. "Mid Infrared Instrument (MIRI) Cooler Subsystem Prototype Demonstration." *Adv. in Cryo. Eng.* 53: 807-814.

EBEX, Collaboration. 2017. "The EBEX Balloon-Borne Experiment - Gondola, Attitude Control, and Control Software." *https://arxiv.org/abs/1702.07020.*

Edwards, J. et al. 2012. "Dual-Polarized Sinuous Antennas on Extended Hemispherical Silicon Lenses." *IEEE Trans. on Ant. Prop.* 60(9): 4082-4091.

ESA. 2016. *CMB Polarisation mission study - CDF summary presentation.* April 15. http://sci.esa.int/trs/57803-cmb-polarisation-study---cdf-summary-presentation/.

—. 2009. *Planck Cooling System.* September 17. http://sci.esa.int/planck/45498-cooling-system/?fbodylongid=2123.

Fargant, G., Dubruel, D., Cornut, M., et al. 2000. "Very wide band telescope for Planck using optical and radio frequency techniques." Edited by J. B. and Jakobsen, P. Breckinridge. *Proc. SPIE.* 69-79.

Glaister, D.S. et al. 2006. "Ball Aerospace 4-6 K space cryocooler." *AIP Conference Proceedings.* 632.

Gloesener, P. 2006. "Large Aluminium Convex Mirror for the Cryo-Optical Test of the Planck Primary Reflector." *Sixth International Conference on Space Optics, Proceedings of ESA/CNES ICSO 2006.* ESTEC, Noordwijk, The Netherlands.

Granet, C. 2001. "Designing classical Dragonian offset dual-reflector antennas from combinations of prescribed geometric parameters." *IEEE Antennas and Propagation Magazine* 43: 100-107.

Henderson, S.W., et al. 2016. "Advanced ACTPol Cryogenic Detector Arrays and Readout." *J. Low Temp Phys.* 184 (3-4): 772-779.

Holland, W. S., et al. 2013. "SCUBA-2: the 10 000 pixel bolometer camera on the James Clerk Maxwell Telescope." *Monthly Notices of the Royal Astronomical Society* 430.4: 2513-2533.

Hu, W. et al. 2003. "Benchmark parameters for CMB polarization experiments." *Phys. Rev. D* 67.

Irwin, K.D. and Lehnert, K.W. 2004. "Microwave SQUID multiplexer." *Applied Physics Letters* 85.11: 2107-2109.

Jasper, L. E. Z., Xaypraseuth, P. 2017. "Data Production on Past and Future NASA Missions." *IEEE Aerospace Conference.* Big Sky, MT, USA.

Kurki-Suonio, E. et al. 2009. "Destriping CMB temperature and polarization maps." *A&A* 506: 1511-1539.

McCormick, H. et al. 2016. "Development of dual-polarization LEKIDs for CMB observations." *Proc. SPIE.*

Niemack, M., et al. 2016. "BFORE: The B-mode Foreground Experiment." *J. Low Temp. Phys.* 184 (3-4): 746-753.

O'Brient, R. et al. 2013. "A dual-polarized broadband planar antenna ad channelizing filter bank for millimeter wavelengths." *Appl. Phys. Lett.* 102.

Padin, S., Staniszewski, Z., Keisler, R., et al. 2008. "South Pole Telescope optics." *Appl. Opt.* 47: 4418-4428.

Pajot, F. et al. 2010. "Planck pre-launch status: HFI ground calibration." *Astronomy & Astrophysics* 520: A10.

Pajot, F. 2018. "Re: Planck Compression." *Private communication.* October 22.

Planck HFI Core Team. 2011. "Planck early results. IV. First assessment of the High Frequency Instrument in-flight performance." *A&A* 536 (A4).

Planck. 2014. "Planck 2013 results. VI. High Frequency Instrument data processing." *A&A* 571 (A6).

Planck. 2018. "Planck 2018 results. III. High Frequency Instrument data processing and frequency maps." *A&A accepted.*

Planck. 2011. "Planck early results. II. The thermal performance of Planck." *A&A* 536 (A2).

Rabb, J. et al. 2013. "NGAS SCW-4K presentation at the 2013 Space Cryogenics Workshop." Girdwood, AK.

Rahlin, A. et al. 2014. "Pre-flight integration and characterization of the SPIDER balloon-borne telescope." *Proc. SPIE.*

Ross, R. 2004. "Estimation of thermal conduction loads for structural supports of cryogenic spacecraft assemblies." *Cryogenics* 44 (6-8): 421-424.

Shirokoff, E. 2011. "The South Pole Telescope bolometer array and the measurement of the secondary Cosmic Microwave Background anisotropy at small scales." Doctoral thesis, UC Berkeley.

Shirron, P. et al. 2012. "Design of the PIXIE adiabatic demagnetization refrigerators." *Cryogenics* 52 (4-6): 140-144.

Shirron, P. et al. 2016. "Thermodynamic performance of the 3-stage ADR for the Astro-H Soft-X-ray Spectrometer instrument." *Cryogenics* 74: 24-30.

Simon, S. M., et al. 2018. "The Advanced ACTPol 27/39 GHz Array." *Journal of Low Temperature Physics* https://doi.org/10.1007/s10909-018-1963-7.

SpaceX. 2015. "Falcon 9 Launch Vehicle Payload User's Guide, Rev 2." October 21.

SPIDER. 2018. "SPIDER: CMB polarimetry from the edge of space." *Journal of Low Temperature Physics* https://doi.org/10.1007/s10909-018-2078-x.

Stahl, H. P., Henrichs, T. 2016. "Multivariable parametric cost model for space and ground telescopes." *Proc. SPIE 9911, Modeling, Systems Engineering, and Project Management for Astronomy VI.* Edinburgh.

Steinbach, B. et al. 2018. *Thermal Kinetic Inductance detectors for ground-based millimeter-wave cosmology.* arXiv:1803.06413.

Suzuki, A., Arnold, K., Edwards, J., et al. 2014. "Multi-chroic dual-polarization bolometric detectors for studies of the cosmic microwave background." *Journal of Low Temperature Physics* 176: 650–656.

Swetz, D. S., Ade, P. A. R., Amiri, M., et al. 2011. "Overview of the Atacama Cosmology Telescope: Receiver, Instrumentation, and Telescope Systems." *ApJS* 194.

Tauber, J. A., et al. 2010. "Planck pre-launch status: The Planck mission." *A&A* 520.

Toulemont, Y., et al. 2004. "The 3.5m all SiC telescope for Herschel." *Proceedings of the 5th International Conference on Space Optics (ICSO 2004).* Noordwijk, Netherlands. 341-348.

Turner, A. et al. 2001. "Silicon nitride Micromesh Bolometer Array for Submillimeter Astrophysics." *Appl. Opt.* 40 (28): 4921-4932.

Wallis, C., et al. 2017. "Optimal scan strategies for future CMB satellite experiments." *MNRAS* 466: 425-442.

Young, K., et al. 2018. "Optical design of PICO: a concept for a space mission to probe inflation and cosmic origins." *Proc. SPIE.* Austin, TX: Space Telescopes and Instrumentation 2018: Optical, Infrared, and Millimeter Wave.